



Structural and optical investigation of pure and Al doped ZnO annealed at different temperatures

A. Sedky¹ · Atif Mossad Ali² · Mansour Mohamed^{1,3}

Received: 28 June 2019 / Accepted: 11 December 2019 / Published online: 17 December 2019
© Springer Science+Business Media, LLC, part of Springer Nature 2019

Abstract

The structural and optical properties of ZnO and Zn_{0.9}Al_{0.1}O (AlZnO) samples annealed in air at different temperatures of (400–900 °C) for 12 h are investigated. It is found that cell parameters, average crystalline diameter and average grain size are affected by both Al and annealing. The ultra violet (UV) absorption coefficient (α) is increased by Al and can be represented by the relation $;\alpha(\text{AlZnO}) \sim 2\alpha(\text{ZnO})$, but it is generally decreased by annealing. Two different types of band gap are obtained for each sample in which their values are higher for AlZnO than that of ZnO. The first band gap is called fundamental energy gap (E_{gh}) and its value above 3 eV, while the second is called optical energy gap (E_{gL}) and its value below 2.75 eV. In addition, the values of E_{gL} (ZnO), E_{gh} (AlZnO) and E_{gL} (AlZnO) are increased by annealing up to 700 °C, followed by a decrease at 900 °C, while the values of E_{gh} (ZnO) are increased by annealing up to 900 °C. Furthermore, a unique energy gap of 3.33 eV is obtained at 312 °C for ZnO and AlZnO. On the other hand, the lattice dielectric constant (ϵ_L), free carrier concentration (N/m^*), dielectric loss ($\tan \delta$), optical conductivity (σ_{opt}) and electrical conductivity (σ_{ele}) are obtained for both series. It is found that ϵ_L is increased by annealing up to 900 °C for both series, while (N/m^*) is increased by annealing for ZnO, but it is decreased for AlZnO. But their values are higher for ZnO than that of AlZnO. Further, the value of ϵ_L (11.26) of the as-prepared ZnO is nearly similar to the value of ϵ_L (11.76) for AlZnO at 900 °C. Although $\tan \delta$ is similar for both series, it is decreased by annealing up to 900 °C for ZnO, and increased for AlZnO up to 700 °C followed by decrease at 900 °C. Similar behavior is obtained for σ_{opt} while the vice is versa for σ_{ele} . The obtained results are interpreted in terms of the variance of carrier concentration, oxygen vacancies and interatomic spacing against annealing temperature and Al content. The present results confirm the semiconducting nature as well as assure that the high photo-response of the investigated samples.

Keywords ZnO · Doping · Thermal annealing · XRD · SEM · Optical properties

✉ A. Sedky
sedky196000@hotmail.com; sedky1960@yahoo.com

¹ Physics Department, Faculty of Science, Assiut University, Assiut, Egypt

² Physics Department, Faculty of Science, King Khalid University, Abha, Saudi Arabia

³ Physics Department, Faculty of Science, Hail University, Hail, Saudi Arabia

1 Introduction

ZnO has attracted much interest due to its versatile properties such as transparency in the visible range, direct band gap, large free-exciton binding energy and absence of toxicity (Gledhill et al. 2009; Shishiyanu et al. 2005; Anas et al. 2007). Three values of energy gap (3.1, 3.2 and 3.3 eV) and free exciton energy of (60–100 mV) have been reported for ZnO at room temperature (Hagemark 1976; Azmi et al. 2005; Srikant and Clarke 1998). The structure of ZnO is similar to GaN, but in contrast, ZnO is available as large bulk and single crystal. Generally, ZnO structure consists of alternating planes, containing tetrahedral coordinated O^{2-} and Zn^{2+} ions, which are stacked alternately along the c -axis. ZnO has a hexagonal structure (space group C6mc) with ideal lattice parameters $a=0.3296$ nm and $c=0.52065$ nm (Kim et al. 2008; Chaari et al. 2011; Matsuoka et al. 1970).

ZnO is an n -type semiconductor due to excess of Zn metal through Zn twice ionization. The excess of Zn gives origin to intrinsic donors in ZnO, and can be assigned either to the interstitial Zn or to the oxygen vacancy (Houabes et al. 2005; Ramanachalam et al. 1995; Secco and Moore 1957; Krøger 1974; Mahan 1983). However, the properties of ZnO are controlled by these intrinsic defects (oxygen vacancies) generated at high temperatures during sintering and annealing (Sedky et al. 2007). During the quenching of the ZnO, these defects are usually annihilated at the grain boundaries. Since this migration process is normally slow as well as thermally activated, these defects are effectively eliminated (Han et al. 2002). It is generally accepted that the localized states of band gap deplete the charge carriers from bulk ZnO on the either side of the grain boundaries, resulting in the formation of Schottky double barriers that control ZnO properties (Madou and Morrison 1989; Bonasewicz et al. 1986; Castro and Aldao 1998).

Extensive research efforts have been directed towards the fabrication of ZnO and its properties investigation. It has been found that the properties of ZnO are closely related to their oxygen vacancies through either filling or ordering. These oxygen vacancies could be also controlled by different dopants such as Ni, Bi, Mn, Ga, Co, Fe and Al (Sedky et al. 2019; Sedky 2018; Greuter and Blatter 1990).

Structural and electrical properties of $Zn_{1-x}Al_xO$ have investigated by Sedky and El-Suheel (2012). It has been reported that Al has no effect on the XRD peaks corresponding to the wurtzite structure of ZnO, while the average crystalline diameter is decreased. Furthermore, the nonlinear coefficient and breakdown field are shifted to lower values, and consequently the conductivity of ZnO grains is improved. Moreover, it is found that Al, close to 10%, reacted with ZnO and caused depressing of the ZnO grain growth. But above 10%, the Al atoms move to the interstitial positions of ZnO lattice.

The optical and electronic properties of ZnO are very sensitive for any variation in the chemical structure of ZnO, which make these compounds having a wide range of applications (Zeyada et al. 2012; Kumari et al. 2018; Nursaadah Ahmad et al. 2018; Shahrokh Abadi et al. 2015). Although ZnO has a wide range in many applications, there is a lack in the data based on thermal stability of ZnO annealed with dopants, especially at high temperature above 500 °C (Ramanachalam et al. 1995; Zhu et al. 2008; Kang et al. 2008; Shan et al. 2004; Kang et al. 2003; Shinde et al. 2006). However, evaluation of optical constants for pure and doped ZnO has a significant importance in optoelectronic and optical applications such as filters, modulators, solar cells, photodiode, switches, etc.

The stability of electrical properties in ZnO has been investigated by ion migration and defects models. They proposed that Zn interstitials can be formed and frozen in the depletion layer during cooling from sintering temperature down to room temperature (Eda et al.

1980; Sato et al. 1980). It is also assumed that some of defects, such as donor-like positive charge and acceptor like negative charge, could be formed in the grain boundary and affect ZnO stability (Gupta et al. 1981; Einzinger 1982). Moreover, some of positive charges Zn^+ and Zn^{++} could be formed in the depletion layer, but these ions could be removed by heat treatments such as thermal annealing (Gupta and Miller 1988). On the other hand, oxygen vacancies formed below the conduction band have been also identified as donor defects and affect the degree of ZnO stability (Klug and Alexander 1962). In addition, the dopant of 3d transition metals such as Al has indirectly confirmed the grain boundary defects beside Zn in the depletion layer.

Based on the above, we tried to eliminate the possible effects of ion migration to the grain boundaries or the reaction of grain boundary defects with ambient oxygen on the ZnO and AlZnO optical properties. Consequently, this study focuses on the influence of annealing at a temperature up to 900 °C on the structural and morphological of the two series through X-ray diffraction (XRD), scanning electron microscope (SEM) characterization. Moreover, a detailed investigation of the optical constants as a result of Al doping and annealing is introduced. The present study reveals significant variations for ZnO and AlZnO series with respect to annealing temperature. Anyhow, by annealing up to 900 °C, we could increase the lattice dielectric constant, fundamental energy gap, and electrical conductivity for pure ZnO, but the optical conductivity and dielectric loss factor are decreased. While annealing of AlZnO generally improve the lattice dielectric constant, dielectric loss factor and optical conductivity, but the fundamental energy gap and electrical conductivity are decreased. However, these results gave us more hooping for ZnO stability optimization through both thermal annealing and doping by transition metals such as Al.

2 Experimental details

ZnO and $Zn_{0.9}Al_{0.1}O$ samples are prepared by using solid-state method through different steps. First, the Al_2O_3 and ZnO powders (purity: 99.999, Aldrich) are mixed together according to the atomic percentages. In the next step, the mixed powders are calcined in air at 1000 °C for 12 h. After that, the pellets of calcined powders are sintered at 1000 °C for 10 h in air. In the final step of the synthesis, the samples are quenched in air at room temperature. However, a range of two similar sets of $Zn_{1-x}Fe_xO$ samples with various x values are synthesized by Sedky et al. (2007). The first set is quenched from the sintering temperature to room temperature, while the second set left in the furnace and slowly cooled to room temperature. Although the wurtzite structure and microstructure of pure ZnO are found to be similar in both cases, the breakdown field and nonlinear coefficient are three times higher in quenching than that of slow cooling. This could be attributed to the oxygen vacancies which are produced by quenching and supporting the potential barrier between ZnO grains. Therefore, in the present case, we prefer quenching than slow cooling. The pellets are divided into four pieces (one piece for as prepared and three pieces for annealing). The thermal annealing process for the studied samples is carried out individually in the furnace at different temperatures (400 °C, 700 °C and 900 °C) for 12 h in air. The structure of the samples is investigated by X-ray diffraction technique (Philips PW-1700) using Cu-K α radiation of wave length (λ)=1.5418 Å at 40 kV and 30 mA settings, and at a diffraction angles range (20°–70°). The morphology of the samples is characterized by using scanning electron microscope (SEM) JSM 5400 LV. The optical absorbance and optical reflectance are collected for the powder suspension of the samples using a thermo-evolution 300 UV

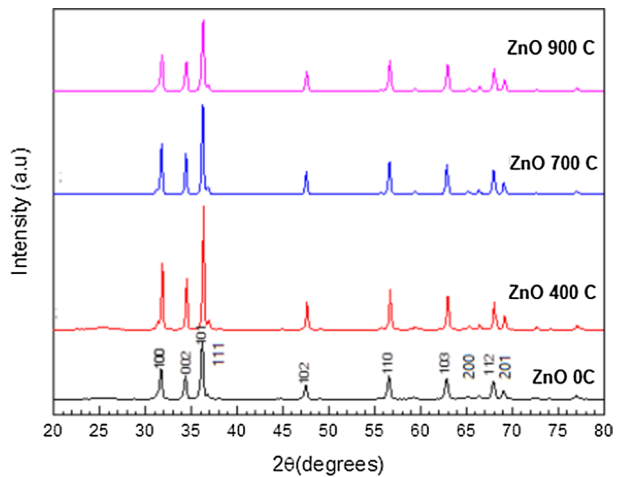
spectrophotometer with a scan speed of 1000 nm/min. The measurements are carried out at room temperature between (200–1000 nm) of photon wavelength.

3 Results and discussions

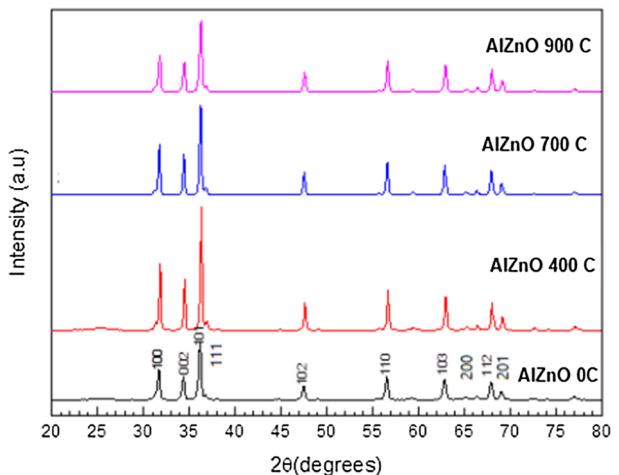
3.1 Structural analysis

The crystal structure of the samples, shown by XRD pattern in Fig. 1a, b, is wurtzite, and no other phases are observed. The density (ρ_{th}) of the samples, calculated using XRD analysis, is given in Table 1. It is clear that the annealing temperature does not affect ρ_{th} for all samples, but their values are generally higher for AlZnO than that of ZnO. The lattice

Fig. 1 X-ray diffraction pattern for undoped **a** ZnO samples, **b** AlZnO samples



(a) X-ray diffraction pattern for undoped ZnO samples



(b) X-ray diffraction pattern for AlZnO samples

Table 1 ρ , D , a , c , u and D versus annealing temperature for ZnO and AlZnO samples

T (°C)	ρ (gm/cm ³)	a (Å)	c (Å)	XRD D_{hkl} (nm)	SEM D (nm)
ZnO					
0	4.338	3.266	5.228	58.76	1711
400	4.324	3.270	5.232	50.10	1903
700	4.341	3.266	5.224	58.27	2262
900	4.343	3.264	5.228	42.11	2371
AlZnO					
0	4.192	3.261	5.221	44.78	693
400	4.201	3.245	5.198	63.16	673
700	4.211	3.256	5.212	58.20	652
900	4.222	3.253	5.208	51.20	666

parameters, summarized in Table 1, are plotted against annealing temperature and shown in Fig. 2a. Although the lattice parameters are nearly unchanged by annealing temperature, their values are lower for AlZnO than that of ZnO. This could be attributed the ionic radius of Al³⁺ (0.51 Å), which is smaller than that of Zn²⁺ (0.74 Å).

The average crystallite size (D_{hkl}) is calculated using the following expression (Klug and Alexander 1962; Cullity and Stock 2001);

$$D_{hkl} = \frac{k\lambda}{\beta \cos \theta} \quad (1)$$

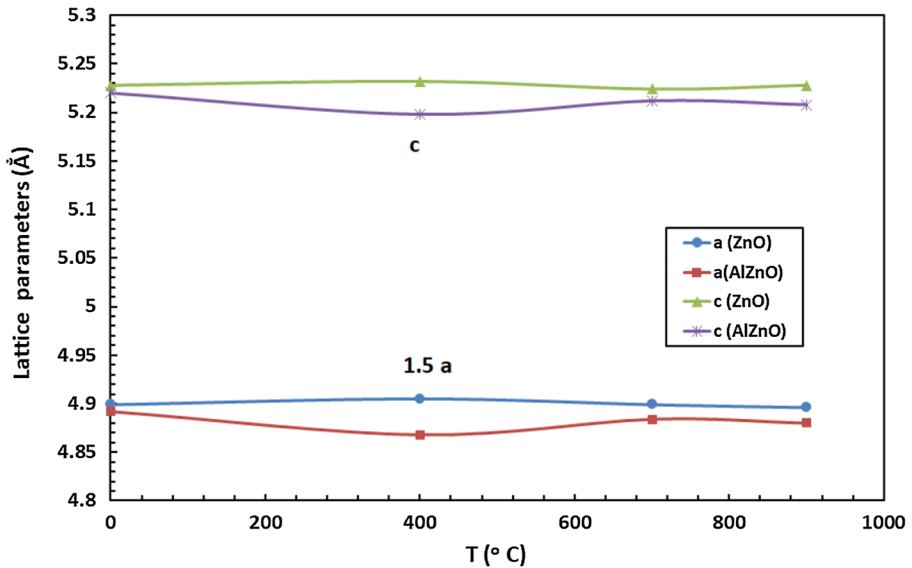
where k is constant and equal 0.93 for ZnO, $\lambda = 1.5418$ Å is the X-ray radiation wave length, β is half maximum line width and θ is diffraction angle. The values of D_{hkl} , summarized in Table 1, are plotted against annealing temperature in Fig. 2b. It is clear that D_{hkl} values decrease by annealing for ZnO and increase for AlZnO. The values of D_{hkl} are ranged between (42.11–58.76 nm) for ZnO, and from (44.78–63.16 nm) for AlZnO.

The morphology of the samples surface is shown in Fig. 3. The surface of the samples is rough and the grains of crystallites having very varied shapes of different sizes which are affected by annealing (see Fig. 3). Furthermore, the crystallites are randomly distributed and irregularly disoriented, and there is no additional phases formed at boundaries of the grain. The AlZnO sample revealed a decrease of the average grain size as compared to ZnO sample at the same annealing temperature. Moreover, the ZnO samples exhibit a uniform granular precipitation on the mother grains without black regions formation. In addition, the size of grains is increased by annealing up to 900 °C. On the other hand, the AlZnO show black regions with random distribution in the matrix structure and the size of grains are relatively small as compared to ZnO. Also, by increasing annealing at 900 °C, the shape of grains became not clear.

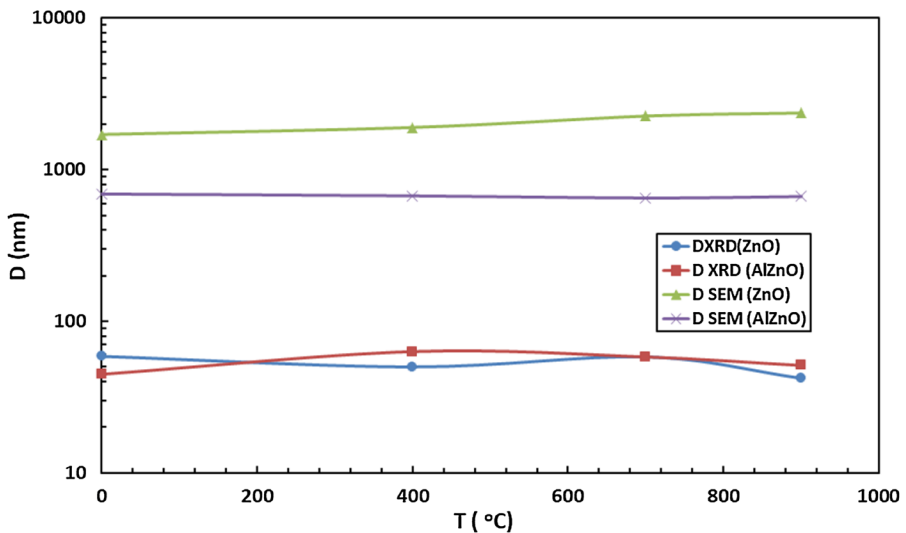
The average size of the grain (D) is determined by the linear intercept method with the help of expression,

$$D = \frac{1.56L}{MN},$$

where L is the length of random line on the micrograph, M is the micrograph magnification, and N is the number of grain boundaries intercepted by the lines (Wurst and Nelson 1972). The values of the average grain size (D) given in Table 1, are plotted against annealing temperature in Fig. 2b. It is found that the values of D are about 13 times



(a) Lattice parameters versus annealing temperature for ZnO and AlZnO samples



(b) Grain size versus annealing temperature for ZnO and AlZnO samples

Fig. 2 a Lattice parameters versus annealing temperature for ZnO and AlZnO samples. b Grain size versus annealing temperature for ZnO and AlZnO samples

higher than D_{hkl} determined from XRD. It is also apparent that average grain sizes are increased by annealing temperature for all studied samples. However, the reported TEM analysis of diluted magnetic semiconductors formed by partial substitution of ZnO with Ni showed that the size of most particles is about 60 nm (Pei et al. 2006). However, D_{hkl} should be smaller than D . This is because XRD analysis determines the average diameter

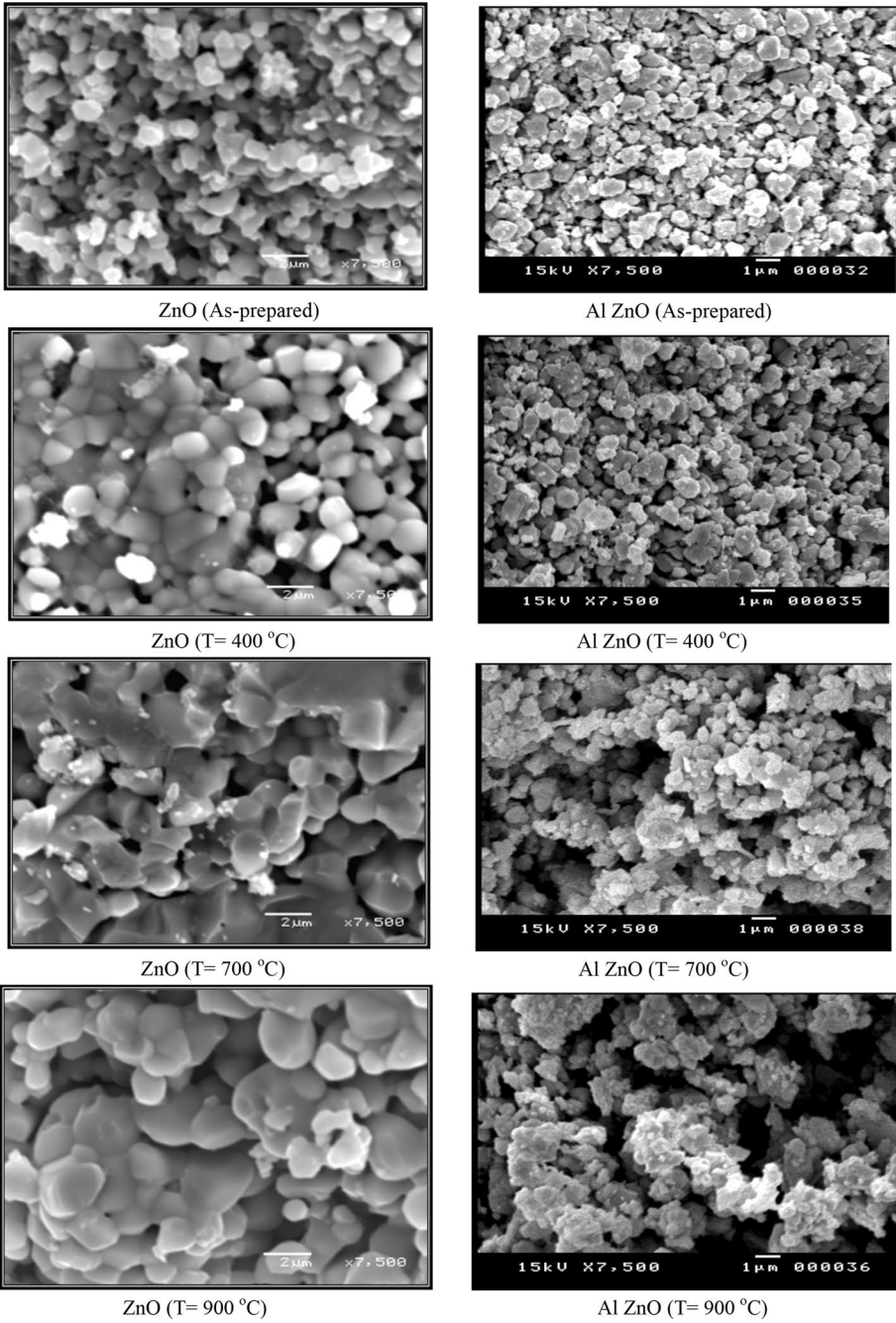


Fig. 3 SEM images of the ZnO and Al ZnO samples

of crystallites which have the same orientation inside the grain, while SEM determines the average size of grain itself. It is well known that each grain contains lot of crystallites with the same orientations.

3.2 Optical measurements and energy gap

The optical absorbance (A) and optical reflectance (R) versus the wavelength are shown in Fig. 4a, b for all samples. A gradual decrease in the absorbance of ZnO with decreasing wavelength occurs. Also, there is an increase of absorbance by increasing photon energy near-infrared region (exciton peaks ~ 400 nm), which can be attributed to an increase of free carrier concentration as the photon energy increases. Furthermore, the absorbance is gradually decreased by increasing annealing temperature up to 900°C . On the other hand, a little bit increase in the absorbance of AlZnO samples with decreasing wavelength is observed. In addition, the values of absorbance of AlZnO are higher than that of ZnO (A of AlZnO $\approx 2 A$ of ZnO). As compared to ZnO, it is observed that the absorbance of AlZnO is almost linear at the longer wavelengths, while it is nonlinear at the lower range of wavelength (300–400 nm). At such wave length range, a number of absorption peaks are recorded, and the intensity and number of these peaks are decreased by increasing annealing temperature. This can be attributed to the free carriers or some defects. Furthermore, the absorbance of AlZnO is increased by increasing annealing temperature up to 700°C , followed by a decrease at 900°C . The vice is versa for optical reflectance R . This behavior may be related to oxygen vacancies and Al interstitials, which makes ZnO very suitable

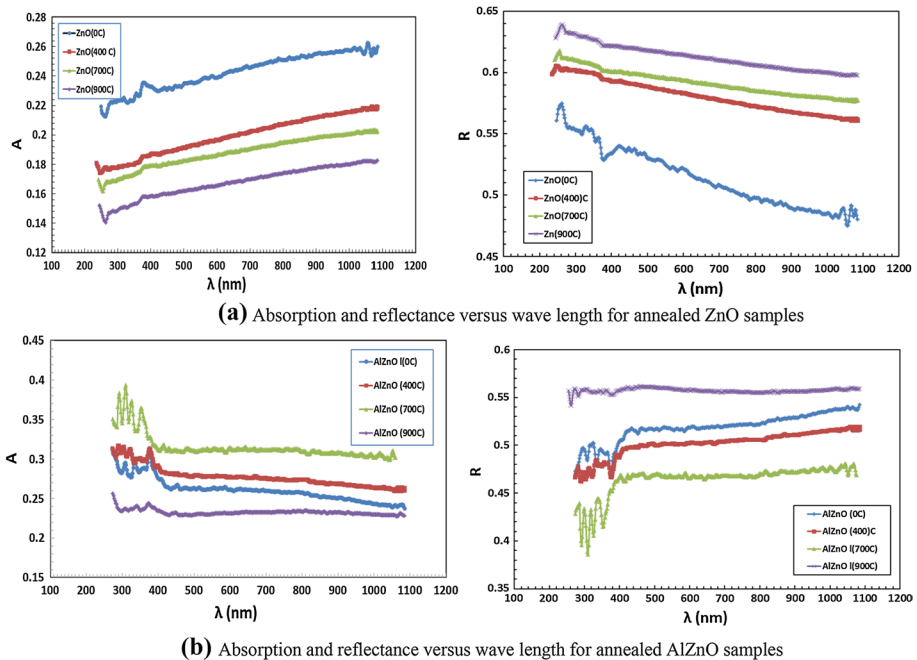


Fig. 4 Absorption and reflectance versus wave length for annealed **a** ZnO samples, **b** AlZnO samples

for the use of oxygen sensor (Fergus 2003). The sensor output depends on the reactions between the defects in the ZnO oxide and the oxygen in the atmosphere (Ali and Abdel Hakeem 2010).

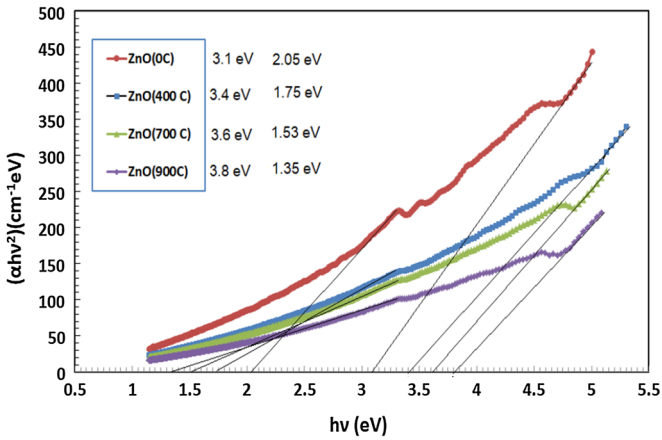
However, ZnO acts as an n-type semiconductor and its conduction band is composed of 4 s orbital of Zn and wide enough for the effective transfer of the charges. Consequently, electrons are excited from the valence state due to absorption of light and generating electron-hole pairs necessary for conduction mechanism. Above the limit of the band gap, the signal of photon energy is due to non-radiative process, and below that limit, it is due to the Urbach tail (Shaaban et al. 2017).

For optical band gap E_g determination, the absorption coefficient α is calculated using the formula, $\alpha = 2.303 \ln(A/t)$, where t is the distance traveled by the photons into the solution of thickness, $t = 12$ mm. After that, E_g is calculated using the following Tauc's equation (Shen and Toyoda 2000):

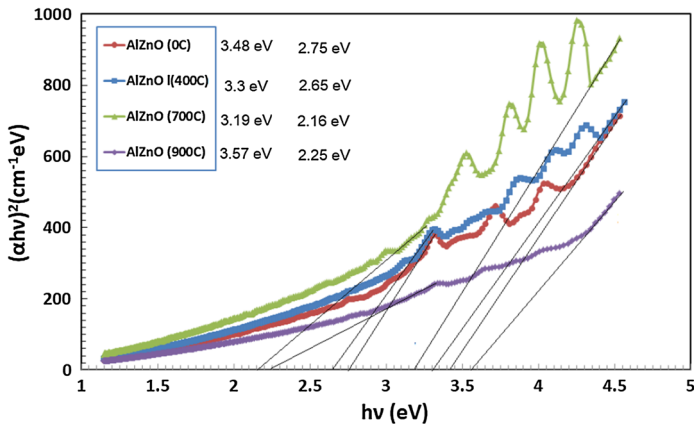
$$(ahv)^{\frac{1}{m}} = A(hv - E_g) \quad (2)$$

A is constant, α is absorption coefficient, ν is photon frequency and h is Planck's constant, respectively. m is a parameter which characterizes the type of electronic transition. It takes 1/2, 2, 1/3, 3 for direct and indirect allowed transition, and 1/3, 3 for direct and indirect forbidden transition, respectively. The present results showed that ZnO possess an allowed direct transition mechanism ($m = 1/2$). This is clearly observed through the exponential like behavior and the linear part characterizing the optical band edge. Therefore, E_g is determined by extrapolating the linear part of the plot of $(ahv)^2$ versus photon energy $h\nu$ to $\alpha = 0$ (Abdalla et al. 2003; Othman et al. 2017). From Fig. 5a for ZnO, one can observe that α values increase as the photon energy increases and it is significantly affected by the increase of annealing temperature up to 900 °C where the absorption edge also shifted to higher energy. While for AlZnO samples, shown in Fig. 5b, an increase in the values of α with increasing annealing temperature up to 700 °C is observed. But with further increase of annealing temperature up to 700 °C, a decrease of the absorption coefficient is occurred. Thus the relation between the values of α between the two series can be represented by; α (AlZnO) $\approx 2\alpha$ (ZnO), indicating that AlZnO is convenient as absorber better than ZnO.

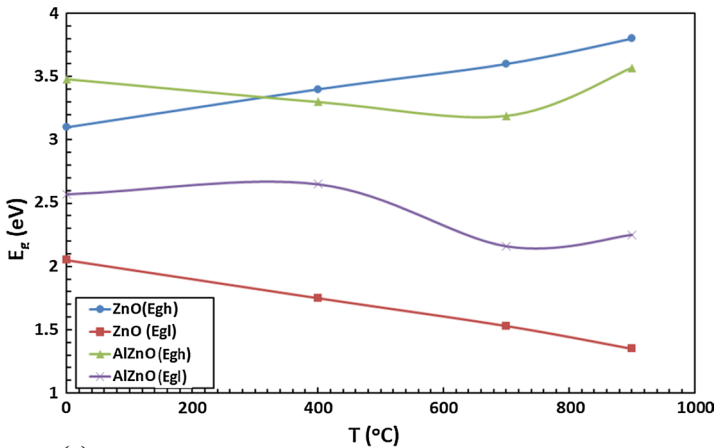
Anyhow, two different values of energy are evident from the plot shown in Fig. 5. The first band gap (E_{gh}) is obtained at higher photon energy (UV region), while the second one (E_{gl}) is obtained at lower photon energy (visible region). The behavior of E_g against annealing temperature for ZnO and AlZnO samples is shown in Fig. 5c, and similar values are summarized in Table 2. It is clear that the values of E_{gh} and E_{gl} are, respectively 3.1, 3.4, 3.5, 3.8 eV, and 2.05, 1.75, 1.53, 1.35 eV for ZnO. This indicates that E_{gh} is increased, whereas E_{gl} is decreased as the annealing temperature increases up to 900 °C. On the other hand, E_{gh} and E_{gl} values for AlZnO are 3.48, 3.3, 3.19, 3.57 eV and 2.75, 2.65, 2.17, 2.25 eV, respectively. This of course means that both E_{gh} and E_{gl} are decreased by increasing annealing temperature up to 700 °C, followed by increase at 900 °C. Although the values of E_g agree with reported for ZnO compound, two optical energy gaps are also reported for n-type semiconductors (Ali et al. 2005; Darzi et al. 2009; Ottaviano et al. 2004; El-Nahass et al. 2016). This can be in principle interpreted in terms of the shape of conduction and valence bands as follows. At higher photon energy and by assuming the geometrical symmetry, the electronic transition could take place from the valence band (VB) top or bottom to conduction band (CB) top or bottom, which is consistent with the higher absorptions values (homo-lumo). But when the phonon energy is decreased, the energy might be not enough for the above transition to occur. Therefore the transition of the electron is only



(a) $(\alpha h\nu)^2$ versus photon energy at annealed ZnO samples



(b) $(\alpha h\nu)^2$ versus photon energy of annealed AlZnO samples



(c) Energy gap versus annealing temperature for ZnO and AlZnO samples

Fig. 5 **a** $(\alpha h\nu)^2$ versus photon energy at annealed ZnO samples. **b** $(\alpha h\nu)^2$ versus photon energy of annealed AlZnO samples. **c** Energy gap versus annealing temperature for ZnO and AlZnO samples

Table 2 E_{gh} , E_{gl} , ΔE , slope, N/m^* , N , R and ϵ_L of studied samples

Annealing temp.	E_{gh} (eV)	E_{gl} (eV)	ΔE (eV)	N/m^* ($g^{-1} cm^{-3}$)	N (cm^{-3})	R (cm)	ϵ_L
ZnO							
As-prepared	3.1	2.05	1.05	3.69×10^{55}	14.09×10^{30}	4.24×10^{-11}	11.26
400	3.4	1.75	1.65	3.81×10^{55}	14.55×10^{30}	4.19×10^{-11}	15.53
700	3.5	1.53	2.15	3.87×10^{55}	14.78×10^{30}	4.17×10^{-11}	16.26
900	3.8	1.35	2.45	4.02×10^{55}	15.36×10^{30}	4.12×10^{-11}	18.55
AlZnO							
As-prepared	3.48	2.75	0.73	1.23×10^{55}	4.70×10^{30}	6.11×10^{-11}	7.44
400	3.30	2.65	0.65	1.11×10^{55}	4.24×10^{30}	6.33×10^{-11}	8.74
700	3.19	2.16	1.03	0.49×10^{55}	1.87×10^{30}	8.31×10^{-11}	9.36
900	3.57	2.25	1.32	0.01×10^{55}	0.04×10^{30}	29.89×10^{-11}	11.74

take place from the top of VB to bottom of CB, which agrees with the lower absorptions values. Generally, this behavior is in a good agreement with the reported data based on n-type semiconductors (El-Denglawey 2018; Yu et al. 2001).

The influence of thermal annealing up to 500 °C on the absorption coefficient of as-deposited semiconducting thin films as a function of photon energy has been investigated (Wang et al. 2003; Abdel-Khalek et al. 2019). Two peaks have been obtained in the UV region; the first at 398.7 nm (3.11 eV) and was red-shifted with increasing annealing temperature, while the second at 279.9 nm (4.43 eV). There is also shoulder exists at 223 nm (5.56 eV) which is attributed to a transition from trap level near the LUMO band to LUMO band (Zeyada et al. 2013). It is approved that the UV emission peaks (300–380 nm) are fundamental and normally resulted from the transfer of electron from conduction band to valence band (Su et al. 1984). While the violet emission peaks close to 450 nm (2.75 eV) are attributed to the transition of electron from conduction band to zinc vacancies (VZn) (Kundu et al. 2011). The blue emissions peaks close to 500 nm (2.48 eV) are attributed to the transition of electron from zinc interstitial (Zn_i) to zinc vacancies (VZn). The green emission close 550 nm (2.25 eV) is attributed to the transition of electron from conduction band to the oxygen anisite vacancy defect (OZn) (Kundu et al. 2011). Therefore, the annealed crystalline films emits UV, violet, blue, and green emissions, but the deposited amorphous film emit UV emission only which indicated that the density of point defect in the annealed film is higher than the deposited at RT. These results strengthens the presence of two energy gap in pure and Al doped ZnO of the present work.

On the other hand, by looking to the behavior of E_{gh} against the annealing temperature, we noted that E_{gh} increased for as-prepared ZnO from 3.1 eV to 3.48 eV for as-prepared AlZnO. The beauty of Fig. 5c that E_{gh} equal 3.33 eV at a temperature of 314 °C for both series. Furthermore, an increase of temperature above 700 °C results an increase of E_{gh} for both samples. While, E_{gl} is generally decreased by increasing annealing temperature up to 900 °C for the two series, but it is always higher for AlZnO, which is completely different than that of E_{gh} behavior.

The crystalline and oxygen vacancies defects have significant effects on the optical band gap of ZnO. The as prepared ZnO sample is usually characterized by structure disorder and normally contains some defects which produce localized states (Lin et al. 2013; Ali and Hakeem 2015). These defects are higher for the as prepared AlZnO, and consequently E_{gh} is 3.48 eV, which is higher than E_{gh} for ZnO (3.1 eV). Additionally, the increase of optical

band gap by Al may be due to decreasing free carrier concentration, thereby resulting in a widening of the band gap which is well-known as Burstein–Moss effect (Burstein 1954). This will be discussed in the next paragraph. Anyhow, the higher values of E_{gh} for ZnO by annealing can be ascribed by structural changes from disordered to ordered structure, which is supported by increasing their crystalline size (1711–2371 nm). The vice is versa for E_{gl} obtained in the visible region. On the other hand, both Al and annealing temperature generally decreased the crystalline size of ZnO (693–652 nm), and consequently E_{gh} decreased by annealing up to 700 °C, followed by an increase at 900 °C. Similar behavior is obtained for E_{gl} .

3.3 Dielectric constant and optical conductivity

The dielectric constant real part (ϵ_1) is determined by using the equation (El-Denglawey 2011; Zaki and El-Amin 2017);

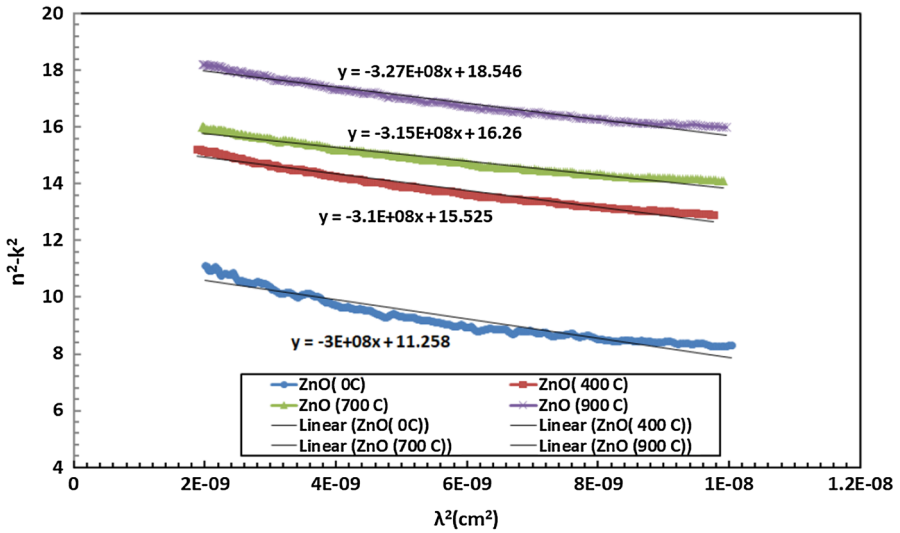
$$\epsilon_1 = n^2 - k^2 = \epsilon_L - \frac{e^2 N}{4\pi^2 \epsilon_0 c^2 m^*} \lambda^2 \quad (3a)$$

where e is the electronic charge, N is concentration of the free carriers, m^* is effective mass, ϵ_0 is permittivity of free space, c is light speed and ϵ_L is residual lattice dielectric constant which represents high frequency component of the relative permittivity at $\lambda=0$. n is refractive index given from the values of reflectance R as follows;

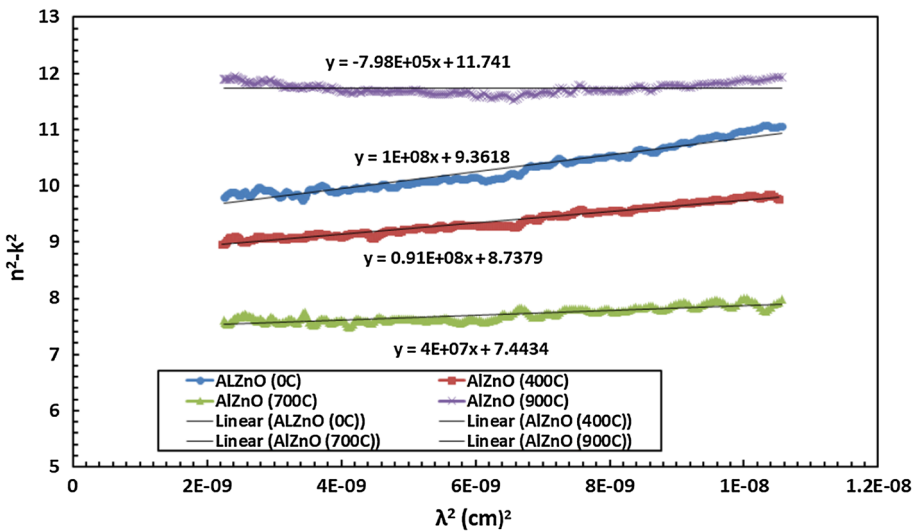
$$n = \frac{1+R}{1-R} + \left(\frac{4R}{(1-R)^2} - K^2 \right)^{\frac{1}{2}} \quad (3b)$$

Figure 6a, b shows the behavior of $(n^2 - k^2)$ against λ^2 at different annealing temperature for the samples. It is observed that this behavior is almost linear at the lower photon energy, while it loses its linearity at the higher energy. N/m^* and ϵ_L are calculated from the slope of linear parts and extrapolation of the plot to $\lambda^2=0$, respectively. The behaviors of (N/m^*) and ϵ_L against annealing temperature for ZnO and AlZnO are shown in Fig. 7a, b, and similar values are listed in Table 2. It is clear that the values of ϵ_L are increased as annealing temperature increases up to 900 °C for both series. While (N/m^*) are increased for ZnO, but it is decreased for AlZnO. In addition, one can see that the value of ϵ_L ($\epsilon_L=11.26$) for the as-prepared ZnO, which is nearly similar that ($\epsilon_L=11.76$) for AlZnO at 900 °C. Furthermore, there is a dramatic decrease in the values of (N/m^*) above 400 °C for AlZnO as compared to the increase for ZnO. By looking to the present results, one can see that the optical energy gap, E_{gh} , and ϵ_L seemed to be changed in the same manner for both series. The increase of free carrier concentration up to 900 °C for ZnO can be achieved to the decrease of oxygen deficiency or electrons. While the decrease of free carrier concentration for AlZnO can be attributed to the increase of holes carriers as a result of substitution of Zn^{2+} by Al^{3+} (Ali and Hakeem 2015). For more clarification, free carrier concentration N is calculated using the average value of m^* which has been reported for ZnO ($m^*=3.82 \times 10^{-25}$ g) (El-Desoky et al. 2014), and therefore the inter-atomic distance (R) can be calculated by using the relation; $R=(1/N^{(1/3)})$ (El-Desoky 2005; Wemple 1973).

The obtained values of N and R are listed in Table 2. It is clear that N is increased by annealing up to 900 °C for ZnO, while it is decreased for AlZnO. The vice is versa for inter-atomic distance R .



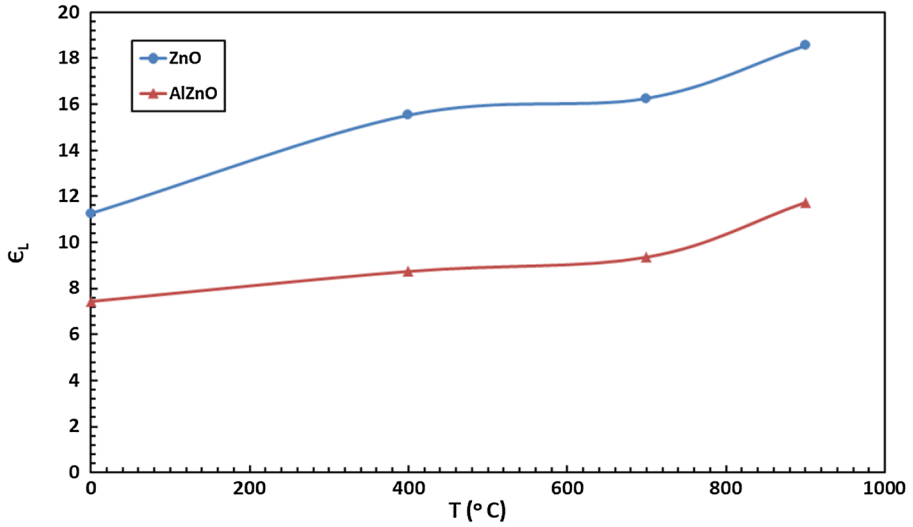
(a) The relation between (n^2-k^2) and λ^2 of annealed ZnO samples



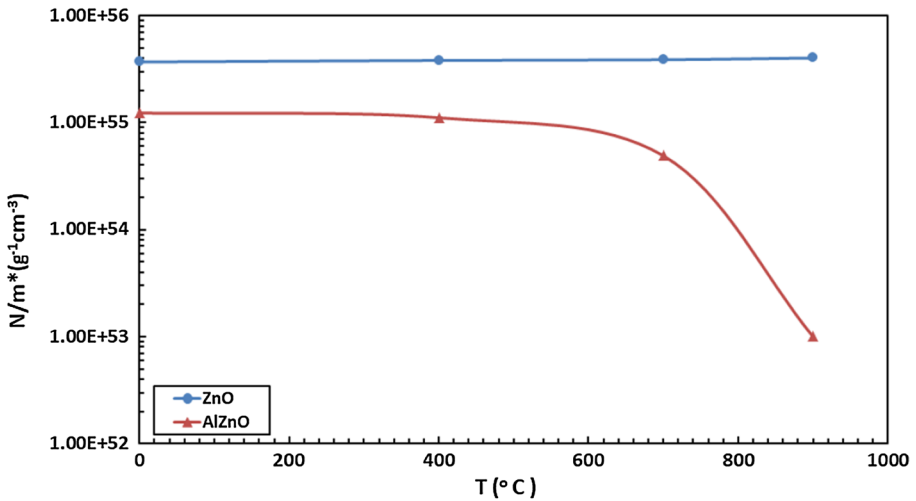
(b) (n^2-k^2) versus λ^2 of annealed AlZnO samples

Fig. 6 **a** The relation between (n^2-k^2) and λ^2 of annealed ZnO samples. **b** (n^2-k^2) versus λ^2 of annealed AlZnO samples

The dielectric constant ϵ is very important optical parameter because it is usually provide information for the electronic structure of materials and helps for its design as optoelectronic devices. The dielectric constant is written as function of the imaginary parts ϵ_1 and ϵ_2 as follows (Swanepoel 1984; Li et al. 2010);



(a) Lattice dielectric versus annealing temperature of ZnO and AlZnO samples

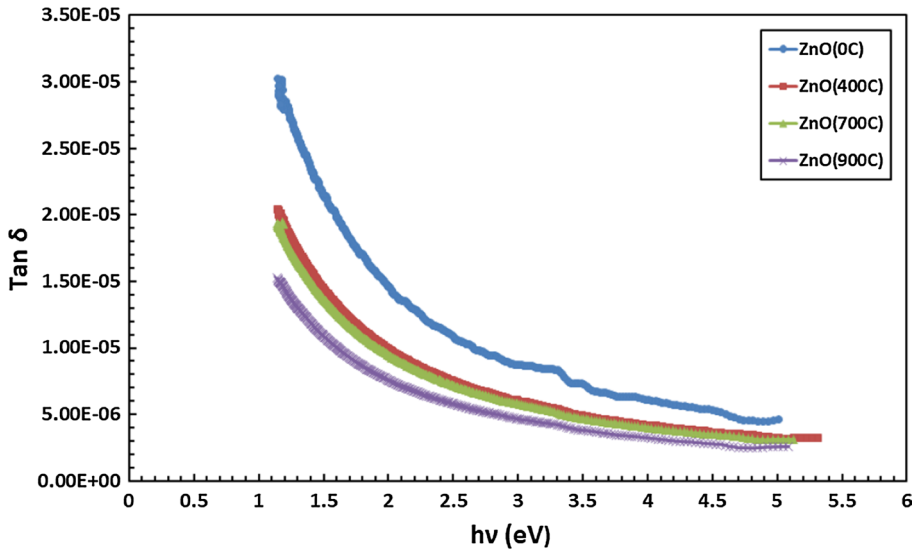


(b) (N/m³) against annealing temperature of ZnO and AlZnO samples

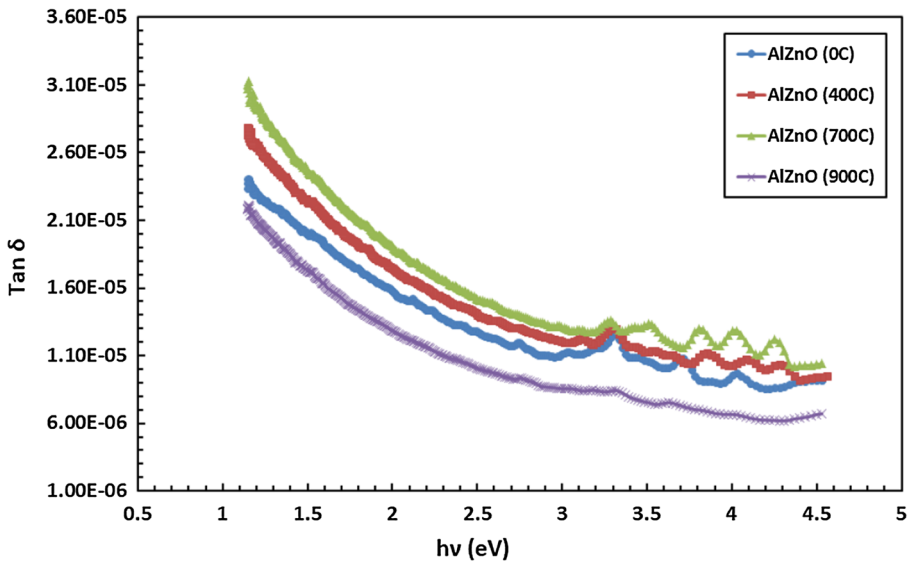
Fig. 7 a Lattice dielectric versus annealing temperature of ZnO and AlZnO samples. b (N/m³) against annealing temperature of ZnO and AlZnO samples

$$\begin{aligned} \epsilon &= \epsilon_1 - i\epsilon_2 \\ \tan \delta &= \frac{\epsilon_2}{\epsilon_1} = \frac{2nk}{n^2 - k^2} \end{aligned} \tag{4}$$

where $\tan \delta$ is the dielectric loss factor generated from the dielectric constant components ϵ_2 and ϵ_1 . These components are given in terms of extinction coefficient (k) and refractive index n . k is responsible for attenuation of light and ϵ_1 is responsible for attenuation



(a) The relation between Dielectric loss and $h\nu$ of annealed ZnO samples



(b) Dielectric loss versus $h\nu$ of annealed AlZnO samples

Fig. 8 a The relation between Dielectric loss and $h\nu$ of annealed ZnO samples. b Dielectric loss versus $h\nu$ of annealed AlZnO samples

of electrical field causing dielectric loss. The relation between $\tan \delta$ and $h\nu$ is shown in Fig. 8a, b. It is found that $\tan \delta$ is almost constant and increases sharply as the photon energy increases. While, it is gradually decreased by annealing up to 900 °C for ZnO, but it is increased for AlZnO up to 700 °C, followed by decrease at 900 °C. The drop of $\tan \delta$

at 900 °C for AlZnO can be attributed to the increase in polarization probability occurred by increasing temperature, in agreement with the reported data (Dongol et al. 2006, 2007).

The optical response is mainly obtained for any material in terms of optical conductivity (σ_{opt}) which is determined using the following formula (Ali and Abdel-Rahim 2013; Girisun and Dhanuskodi 2009);

$$\sigma_{opt} = \frac{\alpha nc}{4\pi} \quad (5a)$$

Also, the electrical conductivity (σ_{ele}) due optical response of the material is given by Ali and Abdel-Rahim (2013) and Girisun and Dhanuskodi (2009)

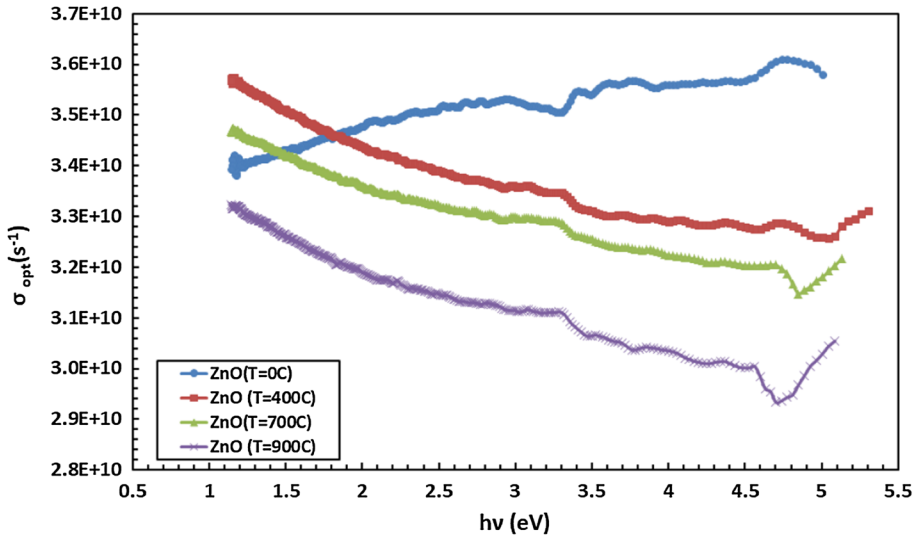
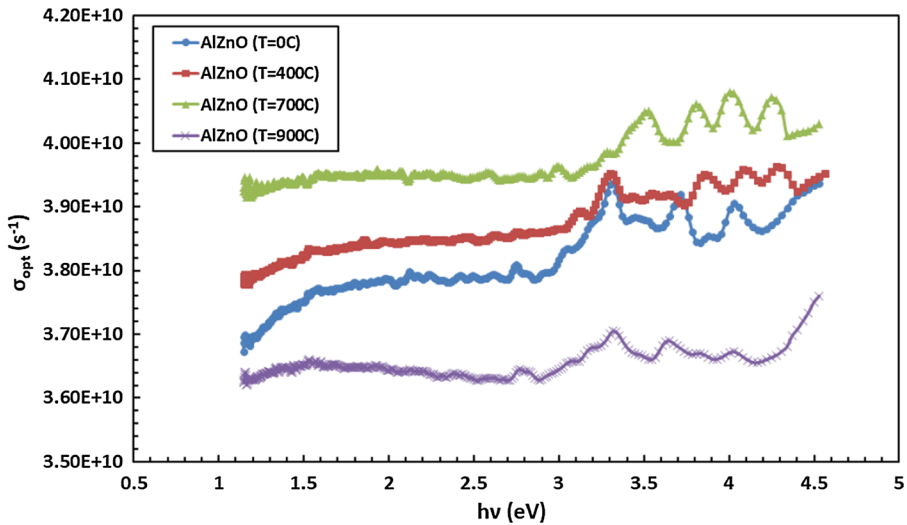
$$\sigma_{ele} = \left(\frac{2\lambda}{\alpha}\right)\sigma_{opt} \quad (5b)$$

The behavior of σ_{opt} against photon energy and at different values of annealing temperature for ZnO and AlZnO is shown in Fig. 9a, b. It is noticed that σ_{opt} decreases by annealing up to 900 °C for ZnO, while it increases up to 700 °C, followed by a decrease at 900 °C for AlZnO. This behavior probably confirms semi-metallic nature up to 700 °C, followed by semiconducting nature at 900 °C. Similar behavior is obtained for the behaviors of σ_{ele} against annealing temperature for ZnO and AlZnO as shown in Figs. 10a, b. However, the higher magnitude of σ_{opt} as the photon energy increases assures the high photo-response of the annealed samples. This behavior is due to the increase of electron excitation by photon energy and annealing temperature (Fouad and El-Radaf 2018; El-Bana and Fouad 2017). It can be also noticed that σ_{ele} increases as the photon energy increases, which confirms the semiconducting nature of the samples (Fouad et al. 2016). Furthermore, the values of σ_{opt} and σ_{ele} for ZnO are slightly higher than that of AlZnO, in agreement with the structural analysis.

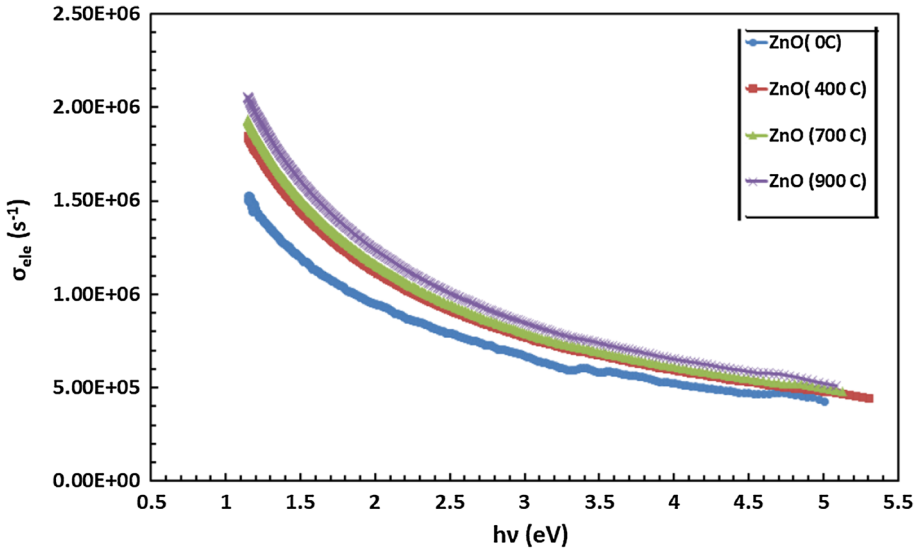
Anyhow, It has been reported that Al reacted with ZnO and formed $ZnAl_2O_4$ on the grain boundaries, and small amount of $ZnAl_2O_4 > 1\%$ depressed the grain growth of ZnO, and can significantly decreased its dielectric constant (Li et al. 2016). Furthermore, it is obtained from our previous work that breakdown field decreased by 0.1 Al, while electrical conductivity is improved. However, for ZnO doped more than 10% Al, Al^{3+} ions tend to move to the interstitial positions of Zn sites. At such interstitial position, the following reaction can be applied; $\frac{1}{2}Al_2O_3 \rightarrow \frac{3}{4}O_2 + Al^* + P$, where an electron is absorbed (Matsuoka et al. 1970; Houabes et al. 2005; Gupta 1992). Al^* is the ionized Al atom in interstitial sites and P is positive hole charge. In this case, the Al acts as an acceptor which dominates the donor effect, resulting in a decrease of the electrical conductivity of ZnO. Furthermore, the structural distortion becomes stronger than relaxation time τ and consequently the conductivity is decreased ($\sigma_{300} \propto n\tau$), n is carrier concentration. These could be the reasons for the variation of the optical properties of AlZnO samples as compared to ZnO ones.

4 Conclusion

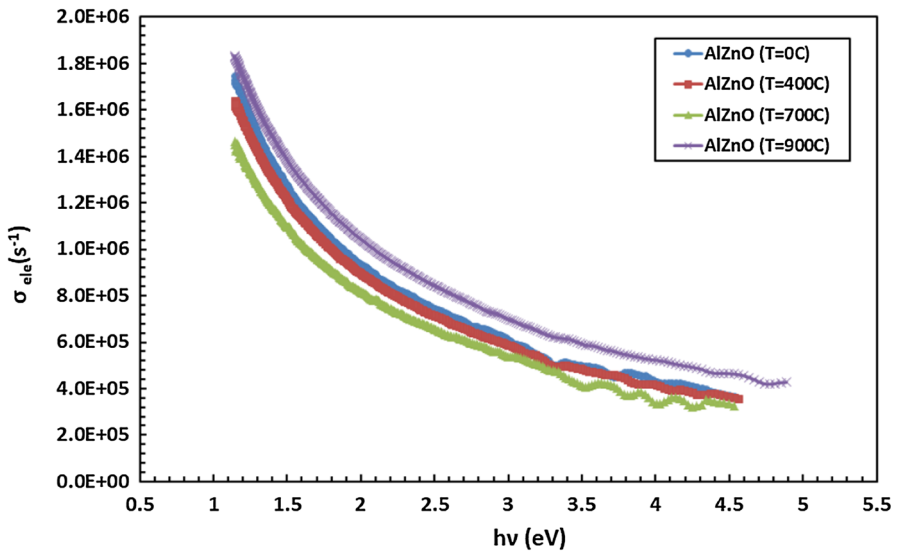
Effect of Annealing temperature on structural and optical investigation of ZnO and $Zn_{0.9}Al_{0.1}O$ is investigated. The cell parameters and average crystalline diameters are affected by both Al and annealing temperature. The ultra violet (UV) absorption coefficient (α) is increased by Al, but it is decreased by annealing, and can be represented by

(a) Optical conductivity versus $h\nu$ of annealed ZnO samples(b) Optical conductivity versus $h\nu$ of annealed AlZnO samplesFig. 9 Optical conductivity versus $h\nu$ of annealed a ZnO samples. b AlZnO samples

the relation: $(\alpha(\text{AlZnO}) \sim 2 \alpha(\text{ZnO}))$ between the two series. Furthermore, $E_{gL}(\text{ZnO})$, $E_{gh}(\text{AlZnO})$ and $E_{gL}(\text{AlZnO})$ are increased by annealing up to 700 °C, followed by a decrease at 900 °C, while $E_{gh}(\text{ZnO})$ is increased up to 900 °C. Moreover, a unique energy gap of 3.33 eV could be obtained at 312 °C for both series. On the other hand, ϵ_L is increased by annealing up to 900 °C for both series, while (N/m^*) is increased for ZnO and decreased for AlZnO. But their values are higher for ZnO than that of AlZnO. Interestingly, the value of ϵ_L (11.26) of the as-prepared ZnO is equal to the value of ϵ_L (11.76) for AlZnO at 900 °C.



(a) Electrical conductivity versus $h\nu$ of annealed ZnO samples



(b) Electrical conductivity versus $h\nu$ of annealed AlZnO samples

Fig. 10 Electrical conductivity versus $h\nu$ of annealed a ZnO samples, b AlZnO samples

Although $\tan \delta$ is similar for both series, it is decreased by annealing up to 900 °C for ZnO, and increased for AlZnO up to 700 °C, followed by decrease at 900 °C. Similar behavior is obtained for σ_{opt} and the vice is versa for σ_{ele} . The obtained results are interpreted in terms of the variance of carrier concentration, oxygen vacancies and interatomic spacing against

annealing temperature and Al content. Moreover, they confirm the semiconducting nature as well as assure that the high photo-response of the investigated samples.

Acknowledgements The authors extend their appreciation to the Deanship of Scientific Research at King Khalid University for funding this work through research groups program under Grant Number R.G.P. 1/121/40.

References

- Abdalla, S., Easawi, K., El-Brollosy, T.A., Yossef, G.M., Negm, S., Talaat, H.: Determination of thermophysical parameters of porous silicon using a photothermal technique. *Rev. Sci. Instrum.* **74**(1), 848–850 (2003)
- Abdel-Khalek, H., Shalaan, E., Abd-El Salam, M., El-Sagheer, A.M., El-Mahalawy, A.M.: Effect of thermal annealing on structural, linear and nonlinear optical properties of 1, 4, 5, 8-naphthalene tetracarboxylic dianhydride thin films. *J. Mol. Struct.* **1178**, 408–419 (2019)
- Ali, H.M., Abdel Hakeem, A.M.: Structural and optical properties of electron-beam evaporated Al₂O₃-doped V₂O₅ thin films for various applications. *Phys. Status Solidi A* **207**(1), 132–138 (2010)
- Ali, K., Abdel-Rahim, F.M.: Effect of Sn addition on the optical constants of Ge–Sb–S thin films based only on their measured reflectance spectra. *J. Alloys Compd.* **561**, 284–290 (2013)
- Ali, H.M., Hakeem, A.M.A.: Characterization of n and p-type (SnO₂)_x(ZnO)_{1-x} nanoparticles thin film. *Eur. Phys. J. Appl. Phys.* **72**, 10301 (2015)
- Ali, H.M., Mohamed, H.A., Mohamed, S.H.: Enhancement of the optical and electrical properties of ITO thin films deposited by electron beam evaporation technique. *Eur. Phys. J. Appl. Phys.* **31**, 87–93 (2005)
- Anas, A., Mangalaraji, R.V., Poothayal, M., Shukla, S.K., Ananthakumar, S.: Direct synthesis of varistor-grade doped nanocrystalline ZnO and its densification through a step-sintering technique. *Acta Mater.* **55**(17), 5792–5801 (2007)
- Azmi, B.Z., Rizwan, Z., Hashim, M., Shaari, A.H., Yunus, W.M.M., Saion, E: Photopyroelectric spectroscopy of MnO doped ceramic ZnO at different sintering temperatures. *Am. J. Appl. Sci. (Special Issue)*, 25–29 (2005). ISSN 1546-9239
- Bonasewicz, P., Hirschwald, W., Newmann, G.: The investigation of the pressure and temperature dependence of the electrical conductivity of thin zinc oxide films with high resistances. *Phys. Status Solidi (a)* **97**, 593–599 (1986)
- Burstein, E.: Anomalous optical absorption limit in InSb. *Phys. Rev.* **93**, 632 (1954)
- Castro, M.S., Aldao, C.M.: Characterization of SnO₂-varistors with different additives. *J. Eur. Ceram. Soc.* **19**, 511–2239 (1998)
- Chari, M., Matoussi, A., Fakhfakh, Z.: Structural and dielectric properties of sintering zinc oxide bulk ceramic. *Mater. Sci. Appl.* **2**, 765–770 (2011)
- Cullity, B.D., Stock, S.R.: *Elements of X-Ray Diffraction*, 3rd edn. Prentice Hall, Upper Saddle River (2001)
- Darzi, S.J., Mahjoub, A.R., Nilehi, A.: Investigation of structural, optical and photocatalytic properties of mesoporous TiO₂ thin film synthesized by sol–gel templating technique. *Phys. E Low Dimens. Syst. Nanostruct.* **42**(1), 76 (2009)
- Dongol, M., El-Nahass, M.M., Abou-Zied, M., El-Denglawey, A.: Effect of Tl addition on the electrical properties of amorphous As₂₀Se_{80-x}Tl_x films. *Phys. B* **371**, 218–222 (2006)
- Dongol, M., El-Nahass, M.M., Abou-Zied, M., El-Denglawey, A.: Thermoelectric properties and mobility activation energy of amorphous As₂₀Se_{80-x}Tl_x films. *Eur. Phys. J. Appl. Phys.* **37**, 257–260 (2007)
- Eda, K., Ega, A., Matsuoka, M.: Degradation mechanism of non-ohmic zinc oxide ceramics. *J. Appl. Phys.* **51**, 2678–2684 (1980)
- Einzinger, R.: Grain boundaries in semiconductors. In: Leamy, H.J., Pike, G.E., Seager, C.H. (eds.) *Grain Boundaries in Semiconductors Symposium, Grain Boundaries in Semiconductors: Proceedings of the Materials Research Society Annual Meeting*, p. 343. Elsevier, New York (1982)
- El-Bana, M.S., Fouad, S.S.: Opto-electrical characterisation of As₃₃Se_{67-x}Sn_x thin films. *J. Alloys Compd.* **695**, 1532–1538 (2017)
- El-Denglawey, A.: Characterization of As–Se–Tl films near infrared region. *Non-Cryst. Solids* **357**, 1757–1763 (2011)

- El-Denglawey, A.: Illumination effect on the structural and optical properties of nano meso nickel (II) tetraphenyl-21H, 23H-porphyrin films induces new two hours photo bleached optical sensor. *J. Lumin.* **194**, 381–386 (2018)
- El-Desoky, M.M.: Characterization and transport properties of V_2O_5 - Fe_2O_3 - TeO_2 glasses. *J. Non-Cryst. Solids* **35**, 139–3146 (2005)
- El-Desoky, M.M., Ali, M.A., Affifi, G., Imam, H.: Annealing effects on the structural and optical properties of growth ZnO thin films fabricated by pulsed laser deposition (PLD). *J. Mater. Sci.: Mater. Electron.* (2014). <https://doi.org/10.1007/s10854-014-2273-8>
- El-Nahass, M.M., Soliman, H.S., El-Denglawey, A.: Absorption edge shift, optical conductivity, and energy loss function of nano thermal-evaporated N-type anatase TiO_2 films. *Appl. Phys. A* **122**, 775 (2016)
- Fergus, J.W.: *J. Mater. Sci.* **38**, 4259–4270 (2003)
- Fouad, S.S., El-Bana, M.S., Sharma, P., Sharma, V.: Effect of compositional dependence on physical and optical parameters of $Te_{17}Se_{83-x}Bi_x$ glassy system. *J. Alloys Compd.* **667**, 204–210 (2016)
- Fouad, S.S., El-Radaf, I.M., Sharma, P.: Multifunctional CZTS thin films: structural, optoelectrical, electrical and photovoltaic properties. *J. Alloys Compd.* **757**, 124–133 (2018)
- Girisun, T., Dhanuskodi, S.: Linear and nonlinear optical properties of tris thiourea zinc sulphate single crystals. *Cryst. Res. Technol.* **44**, 1297–1302 (2009)
- Gledhill, S., Grimm, A., Allsop, A., Koehler, T., Camus, C., Lux-steiner, L., Fisher, C.H.: A spray pyrolysis route to the undoped ZnO layer of Cu(In, Ga)(S, Se)₂ solar cells. *Thin Solid Films* **517**(7), 2309–2311 (2009)
- Greuter, F., Blatter, G.: Electrical properties of grain boundaries in polycrystalline compound semiconductors. *Semicond. Sci. Technol.* **5**, 111 (1990)
- Gupta, T.K.: Microstructural engineering through donor and acceptor doping in the grain and grain boundary of a polycrystalline semiconducting ceramic. *J. Mater. Res.* **7**(12), 3280–3295 (1992)
- Gupta, T.K., Miller, A.C.: Improved stability of the ZnO varistor via donor and acceptor doping at the grain boundary. *J. Mater. Res.* **3**(4), 745–754 (1988)
- Gupta, T.K., Carlson, W.G., Hower, P.L.: Current instability phenomena in ZnO varistors under a continuous ac stress. *J. Appl. Phys.* **52**, 4104–4111 (1981)
- Hagemark, K.: Defect structure of Zn-doped ZnO. *J. Solid State Chem.* **16**, 293–299 (1976)
- Han, J., Senos, A.M.R., Mantas, P.Q.: Deep donors in polycrystalline Mn-doped ZnO. *Mater. Chem. Phys.* **75**, 117–120 (2002)
- Houabes, M., Bernik, S., Talhi, C., Bui, A.: The effect of aluminium oxide on the residual voltage of ZnO varistors. *Ceram. Int.* **29**(6), 783–789 (2005)
- Kang, H.S., Kang, J.S., Pang, S.S., Shim, E.S., Lee, S.Y.: Variation of light emitting properties of ZnO thin films depending on post-annealing temperature. *Mater. Sci. Eng., B* **102**, 313–316 (2003)
- Kang, S.J., Joung, Y.H., Shin, H.H., Yoon, Y.S.: Effect of substrate temperature on structural, optical and electrical properties of ZnO thin films deposited by pulsed laser deposition. *J. Mater. Sci. Mater. Electron.* **19**, 1073–1078 (2008)
- Kim, H.S., Lugo, F., Pearton, S.J., Norton, D.P., Wang, Y.L., Ren, F.: Dielectric passivation effects on ZnO light emitting diodes. *Appl. Phys. Lett.* **92**(11), 112108 (2008)
- Klug, H., Alexander, L.: *X-Ray Diffraction Procedures for Polycrystalline and Amorphous Materials*, p. 125. Wiley, New York (1962)
- Kröger, F.A.: The chemistry of imperfect crystals: preparation, purification, crystal growth and phase theory. *Chem. Imperfect Cryst.* **2**, 743 (1974)
- Kumari, Neelam, Naqvi, Samya, Kumar, Rachana: Naphthalene diimide self-assembled ribbons with high electrical conductivity and mobility without doping. *J. Mater. Sci.* **53**, 4046–4055 (2018)
- Kundu, T.K., Barik, N.K.P., Saha, S.: Annealing effects on the structural and optical properties of growth ZnO thin films fabricated by pulsed laser deposition (PLD). *Int. J. Soft Comput. Eng. (IJSCE) I(NCRAMT2011)*, ISSN: 2231-2307 (2011)
- Li, Y., Xu, L., Li, X., Shena, Wang, A.: Effect of aging time of ZnO sol on the structural and optical properties of ZnO thin films prepared by sol-gel method. *Appl. Surf. Sci.* **256**, 45439–45447 (2010)
- Li, X., Cao, X., Xu, L., Liu, L., Wang, Y., Meng, C., Wang, Z.: High dielectric constant in Al-doped ZnO ceramics using high-pressure treated powders. *J. Alloys Compd.* **675**, 90–94 (2016)
- Lin, C.P., Chen, H., Nakaruk, A., Koshy, P., Sorrell, C.C.: Effect of annealing temperature on the photocatalytic activity of TiO_2 thin films. *Energy Procedia* **34**, 627–636 (2013)
- Madou, J.M., Morrison, R.S.: *Chemical Sensing with Solid State Devices*, vol. 3, p. 12. Academic Press, San Diego (1989)
- Mahan, G.D.: Intrinsic defects in ZnO varistors. *J. Appl. Phys.* **54**, 3825–3832 (1983)
- Matsuoka, M., Masuyama, T., Iida, Y.: Non-linear electrical properties of zinc oxide ceramics. *Suppl. J. Jpn. Soc. Appl. Phys* **39**, 94 (1970)

- Nursaadah Ahmad, P.O.A.D., Siti, Z.N.D., Muhd, Z.Y., Noriah, B.: Optical characteristics of ITO/NTCDA film for defence technology application. *Int. J. Cur. Res. Eng. Sci. Tech.* **1**(S1), 262 (2018)
- Othman, A.A., Othman, M.A., Ibrahim, E.M.M., Ali, M.A.: Sonochemically synthesized ZnO nanosheets and nanorods: annealing temperature effects on the structure, and optical properties. *Ceram. Int.* **43**, 527–533 (2017)
- Ottaviano, L., Pennisi, A., Simone, F., Salvi, A.M.: RF sputtered electrochromic V_2O_5 films. *Opt. Mater.* **27**, 307 (2004)
- Pei, G., Xia, C., Cao, S., Zhang, J., Wu, F., Xu, J.: Synthesis and magnetic properties of Ni doped zinc oxide powders. *J. Magn. Mater.* **302**(2), 340–342 (2006)
- Ramanachalam, M.S., Rohatgi, A., Carter, W.B., Schaffer, J.P., Gupta, T.K.: Photoluminescence study of ZnO varistor stability. *J. Electron. Mater.* **24**(4), 413–419 (1995)
- Sato, K., Takada, Y., Makewa, H., Ototake, M., Tominga, S.: Electrical conduction of ZnO varistors under continuous DC stress. *Jpn. J. Appl. Phys.* **19**, 909 (1980)
- Secco, E.A., Moore, W.J.: Diffusion and exchange of zinc in crystalline zinc oxide. *J. Chem. Phys.* **26**, 942–948 (1957)
- Sedky, A.: Effect of temperature magnetic dopants on particle size and electrical properties of ZnO ceramic varistor. *Adv. Mater. Sci. Eng.* **2**(1), 1 (2018)
- Sedky, A., El-Suheel, E.: Structural and I–V characteristics in pure and doped ZnO varistors. *Chin. Phys. B* **21**(11), 116103 (2012)
- Sedky, A., Abu-Abdeen, M., Almulhem, A.A.: Nonlinear I–V characteristics in doped ZnO based-ceramic varistor. *Phys. B* **388**, 266–273 (2007)
- Sedky, A., Amin, S.A., Mohamed, M.: Electrical, photoluminescence and ferromagnetic characterization of pure and doped ZnO nanostructures. *Appl. Phys. A* **125**, 308 (2019)
- Shaaban, E.R., Soraya, M.M., Shapaan, M., Shokry Hassan, H., Samar, M.M.: Applying wedge shape model for calculating both film thickness and optical constants of $SeSZn$ films with high precision for optoelectronic devices. *J. Alloys Compd.* **693**, 1052–1060 (2017)
- Shahrokh Abadi, M.H., Delbari, A., Fakoor, Z., Baedi, J.: Effects of annealing temperature on infrared spectra of SiO_2 extracted from rice husk. *J. Ceram. Sci. Technol.* **6**, 41–46 (2015)
- Shan, F.K., Liu, Z.F., Liu, G.X., Lee, W.J., Lee, G.H., Kim, I.S.: Aging and annealing effects of ZnO thin films on GaAs substrates deposited by pulsed laser deposition. *J. Electroceram.* **13**, 195–200 (2004)
- Shen, Q., Toyoda, T.: Dependence of the photoacoustic signal intensity on modulation frequency for $CdIn-GaS_4$ crystals under a transmission detection configuration. *Jpn. J. Appl. Phys.* **39**, 3146 (2000)
- Shinde, V.R., Gujar, T.P., Lokhanade, C.D., Mane, R.S., Han, S.H.: Mn doped and undoped ZnO films: a comparative structural, optical and electrical properties study. *Mater. Chem. Phys.* **96**, 326–330 (2006)
- Shishiyanu, S.T., Shishiyanu, T.S., Lupan, O.I.: Sensing characteristics of tin-doped ZnO thin films as NO_2 gas sensor. *Sens. Actuators B Chem.* **107**(1), 379–386 (2005)
- Srikant, V., Clarke, D.R.: On the optical band gap of zinc oxide. *J. Appl. Phys.* **83**(10), 5447–5451 (1998)
- Su, L.M., Grote, N., Schmitt, F.: Diffused planar InP bipolar transistor with a cadmium oxide film emitter. *Electron. Lett.* **20**, 717 (1984)
- Swanepoel, R.: Determination of surface roughness and optical constants of inhomogeneous amorphous silicon films. *J. Phys. E: Sci. Instrum.* **17**, 896 (1984)
- Wang, Y.G., Lau, S.P., Lee, H.W., Yu, S.F., Tay, S.K., Zang, X.Z., Hing, H.H.: Photoluminescence study of ZnO films prepared by thermal oxidation of Zn metallic films in air. *J. Appl. Phys.* **94**, 354–358 (2003)
- Wemple, S.H.: Refractive-index behavior of amorphous semiconductors and glasses. *Phys. Rev. B* **7**, 3767 (1973)
- Wurst, J.C., Nelson, J.A.: Lineal intercept technique for measuring grain size in two-phase polycrystalline ceramics. *J. Am. Ceram. Soc.* **55**(2), 109–109 (1972)
- Yu, J., Zhao, X., Zhao, Q.: Photocatalytic activity of nanometer TiO_2 thin films prepared by the sol–gel method. *Mater. Chem. Phys.* **69**, 25–29 (2001)
- Zaki, A.A., El-Amin, A.A.: Effect of cell thickness on the electrical and optical properties of thin film silicon solar cell. *Opt. Laser Technol.* **97**, 71–76 (2017)
- Zeyada, H.M., EL-Nahass, M.M., El-Ashmawi, I.S., Habashi, A.A.: Annealing temperatures induced optical constant variations of methyl violet 2B thin films manufactured by the spin coating technique. *J. Non-Cryst. Solids* **358**, 625–636 (2012)
- Zeyada, H.M., EL-Nahass, M.M., El-Ashmawi, I.S., Habashi, A.A.: Effect of substitution group variation on the optical functions of 5-sulfono-7-(4-x phenyl azo)-8-hydroxy quinoline thin films. *Curr. Appl. Phys.* **13**(9), 1960–1966 (2013)
- Zhu, B.L., Sun, X.H., Zhao, X.Z., Su, F.H., Li, G.H., Wu, X.G.: The effects of substrate temperature on the structure and properties of ZnO films prepared by pulsed laser deposition. *Vacuum* **82**, 495–500 (2008)